AIMS Environmental Science

AIMS Environmental Science, 13(1): 159–178.
DOI: 10.3934/environsci.2026007
Received: 29 September 2025
Revised: 20 December 2025
Accepted: 12 February 2026
Published: 28 February 2026

http://www.aimspress.com/journal/environmental

Research article

Stability assessment of falling-type unstable rock mass based on amplitude ratio and frequency ratio

LI Hongqiang[1], ZHAO Chen[2,*], ZOU Zinan[1], JIANG Song[2], XIE Mowen[3] and ZHANG Xueliang[4]

[1] PowerChina Chengdu Engineering Corporation Limited, Chengdu 611130
[2] School of Future Cities, University of Science and Technology Beijing, Beijing,100083, China
[3] School of Resources and Safety Engineering, University of Science and Technology Beijing, Beijing 100083, China
[4] China Geo-Engineering Corporation, Beijing 100093

* **Correspondence:** Email: grea_zc@163.com.

Abstract: Due to micro-deformation, wide spatial distribution, and high randomness of instability, stability assessment and early warning of slope rock mass remain challenging. To identify highly sensitive and robust indicators of rock mass damage, we investigated time–frequency dynamic differences between unstable rock mass and bedrock during failure, focusing on micro-vibration characteristics. We further examined their correlation with structural plane constraint strength. Our results showed that the degree of structural plane damage in unstable rock mass is positively correlated with the amplitude ratio between rock mass and bedrock, and negatively correlated with the frequency ratio. By integrating these dynamic indicators with classification algorithms, a dynamics-PSO-SVM-based stability analysis method for unstable rock mass was proposed. This model enabled rapid classification of rock mass stability states based on dynamic indicators. Laboratory-scale similarity experiments analyzed the evolution of amplitude and frequency ratios during rock mass instability, revealing stage-specific patterns in unstable rock mass. The method achieved 100% classification accuracy between stable and unstable states. Moreover, it effectively reduced interference from complex environmental excitation and equipment temperature drift in vibration monitoring data, demonstrating strong noise immunity. These findings enhance the practical applicability of dynamic evaluation methods for assessing the stability of unstable rock mass.

Keywords: falling-type unstable rock mass; stability analysis; amplitude ratio; frequency ratio; PSO–SVM

1. Introduction

Rockfall hazards on slopes, marked by widespread distribution, high concealment, and sudden onset, present significant challenges for identification and stability assessment, often leading to more severe risks and substantial loss of life and property [1]. Among collapse hazards, rockfall is particularly challenging to identify and has severe consequences. Rock mass tumble freely down steep slopes, moving at high speeds and over significant distances. Conventional qualitative or semi-quantitative stability assessment methods rely mainly on surface characteristics of unstable rock mass, such as morphological features, joint combinations, and spatial distribution, but often fail to account for internal damage in joints. Stability assessments based on deformation indicators [2], such as inclination angle, dip direction, and joint opening, are typically effective for slopes exhibiting creep behavior. However, these methods are less effective for evaluating the stability of brittle failure in rigid, jointed rock mass. An accurate assessment of rock mass stability is crucial for developing effective mitigation strategies.

In recent years, stability analysis methods based on dynamic characteristics have gained increasing attention. Several scholars have studied the dynamic response of slopes induced by environmental vibrations, revealing a correlation between rock mass stability and its dynamic characteristics [3,4]. For instance, Du Yan et al.[5] combined the vibration equation of unstable rock mass to investigate the relationship between natural frequency and the bonding area of unstable rock mass, establishing a stability evaluation model based on natural frequency. Zhang Xiaoyong et al.[6,7] developed a quantitative relationship between natural frequency and the depth of rear-edge fractures in unstable rock mass, using it to create a dynamic stability coefficient model based on natural frequency. Zhao Chen et al. [8] analyzed the temporal dynamics of spatial particle trajectory indicators during the evolution of unstable rock mass through collapse similarity model tests, validating the use of particle trajectory dynamics for rock mass damage identification. Jia Yanchang et al .[9] developed a stability evaluation model for unstable rock mass based on natural frequencies, eliminating the need for direct measurement of dominant structural plane parameters during quantitative stability assessments.

Bottelin et al. [10] analyzed the frequency variation characteristics before and after the reinforcement of columnar limestone, finding that the natural frequency of the rock mass increased following reinforcement. Burjánek et al. [11] observed that the direction of amplitude amplification in unstable rock mass correlates with the evolution direction of rear-edge fractures. Kleinbrod [12] classified unstable rock mass into volume-controlled and depth-controlled types by analyzing variations in microtremor characteristics across sites.

Evaluation methods for dynamic indicators primarily focus on monitoring the vibration characteristics of unstable rock mass. However, in complex environmental excitation scenarios (such as traffic, strong winds, or construction disturbances), the vibration characteristics of unstable rock mass fluctuate significantly due to variations in environmental stimuli. Additionally, in high-temperature differential environments, vibration sensors often experience data fluctuations caused by the equipment's own "temperature drift," which affects the accuracy of dynamic evaluation results. In this study, we focus on the differential vibration characteristics between unstable rock mass and bedrock. Using rockfall-prone mass as the research subject, we investigate the evolutionary patterns

of amplitude and frequency ratios between unstable rock mass and bedrock during the instability process. By integrating machine learning algorithms, we explore adaptive stability identification for rockfall-prone mass, thereby enhancing the practicality of dynamic stability evaluation methods for unstable rock mass in complex noise environments.

2. Analysis of vibration characteristics in unstable rock mass and bedrock

The slope rock mass is treated as a rigid body with mass M. The rock bridge divides the slope into bedrock M_1 and unstable rock mass M_2. Based on vibrational dynamics, the constraint at the bonded section of the rock bridge is modeled as a coupled spring-damper system. The constraints on the rock mass are primarily governed by the bonded section of the rock bridge. The unstable rock mass can be simplified as a mass-spring-damper vibration system [13]. A vibration model for the interaction between the unstable rock mass and bedrock is established, as shown in Figure 1.

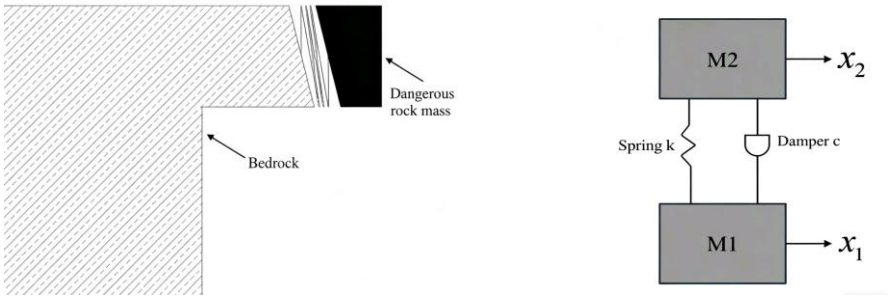

Figure 1. Simplified vibration model for falling rock mass.

Considering vibrations along the normal direction of the rock mass structural plane, when the bedrock M_1 vibrates at $x = a \bullet e^{ipt}$, the vibration equation for the unstable rock mass is expressed by Eq (1):

$$m_2 \ddot{x} + c \ddot{x}_2 + kx_2 = kx_1 + c x_1 \tag{1}$$

In the equation, m_2 represents the mass of the unstable rock mass; x_1 and x_2 represent the displacements of bedrock M_1 and the unstable rock mass M_2, respectively; k is the stiffness of the bonded segment; and c is the damping of the bonded segment.

The amplitude ratio and natural frequency ratio (referred to as the frequency ratio) are defined as shown in Eqs (2) and (3):

$$\mathrm{R} = \frac{\mathrm{b}}{\mathrm{a}} \tag{2}$$

$$\lambda = \frac{\omega_2}{\omega_1} \tag{3}$$

In the formula: R is the amplitude ratio; a is the maximum amplitude of the bedrock; b is the maximum amplitude of the unstable rock mass; λ is the natural frequency ratio; ω_1 is the natural frequency of the bedrock; and ω_2 is the natural frequency of the unstable rock mass, $\omega = \sqrt{\frac{k}{m}}$.

Solving Eq (1) yields the amplitude b of M_2 as:

$$\mathrm{b} = \mathrm{a}\sqrt{\frac{1+(2\xi\lambda)^2}{(1-\lambda^2)^2+(2\xi\lambda)^2}} \tag{4}$$

In the formula, $\tilde{\zeta} = \frac{c}{2\sqrt{km_2}}$ represents the damping ratio of the unstable rock mass.

The vibration of rock mass induced by excitation forces can be regarded as an elastic wave propagation process. When elastic waves propagate from bedrock to unstable rock mass through rock bridges, the dampers within the bonded sections of the rock bridges absorb minimal energy from the vibrating system. Neglecting the damping effect of the rock bridges simplifies the vibration of unstable rock mass to an undamped forced vibration. The damping ratio of rock mass structures typically ranges between 0 and 1, indicating a weakly damped state. Under weakly damped conditions, system vibrations are confined to decaying oscillations within the curve. Since the damping ratio of rock mass structures is generally <<1, we neglect the influence of damping on the natural vibration frequency and maximum amplitude under constant microtremor conditions[14,15]. The amplitude ratio and frequency ratio between the unstable rock mass and bedrock can be expressed as:

$$\begin{cases} R = \dfrac{b}{a} = \left|\dfrac{1}{\lambda^2-1}\right| = \left|\dfrac{1}{\dfrac{\omega^2 m_2}{k}-1}\right| \\ \lambda = \sqrt{\dfrac{k}{m_2\omega_1}} \end{cases} \tag{5}$$

Figure 2 shows the correlation curve between the dynamic index of unstable rock mass and the height of rock bridges. The amplitude ratio exhibits an inverse proportional relationship with stiffness. As stiffness increases, the vibration amplitudes of the unstable rock mass and bedrock tend to converge, with the amplitude ratio approaching 1. The bedrock vibration characteristics on the slope manifest as long-period pulsations, with the bedrock's natural frequency regarded as a stable constant. Consequently, as the instability of the rock mass intensifies, the structural plane stiffness k decreases, and the frequency ratio declines in an approximately exponential trend.

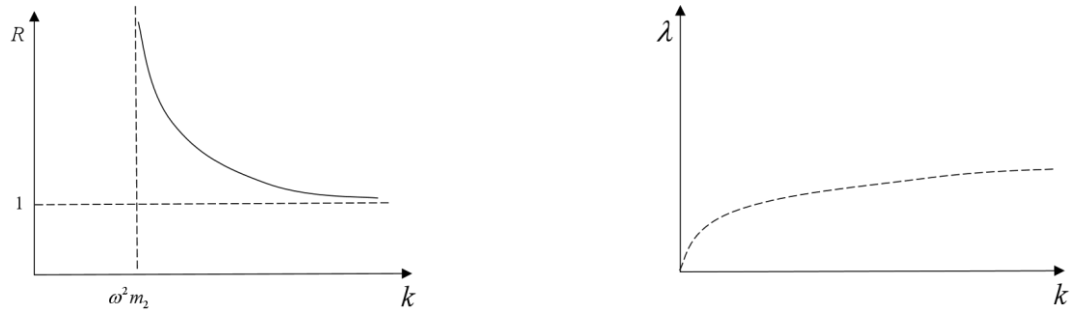

(a) Correlation between amplitude ratio and stiffness index

(b) Frequency ratio-stiffness index correlation

Figure 2. Indicator change diagram.

The vibration amplitude of unstable rock mass on slopes is sensitive to excitation forces such as traffic loads, construction disturbances, and wind loads. Additionally, in high-temperature differential environments, monitoring sensors often exhibit fluctuations in data due to the inherent characteristics of the equipment components, known as "temperature drift"[16], which contaminates the true vibration data of the rock mass. This affects the accuracy of stability evaluation results. The amplitude ratio metric mitigates amplitude fluctuations caused by variations in excitation forces and equipment temperature drift. This is because changes in excitation force simultaneously affect bedrock and unstable rock amplitudes. Compared to monitoring only the time-frequency dynamics of the unstable rock, the ratio of unstable rock to bedrock vibration characteristics provides greater robustness in practical applications by reducing the impact of excitation force variations and equipment temperature drift.

3. Similarity model testing research

The instability of unstable rock mass on slopes often results from prolonged geological evolution, making it challenging to identify precursory patterns of rock mass failure through in-situ monitoring. To capture vibration data throughout the entire damage-evolution-instability process of unstable rock mass, we designed a controlled damage evolution model experiment. By sequentially cutting the rear-edge fractures (Figure 5), the equivalent constraint stiffness k of the rock bridge is reduced, aiming to replicate the natural fracture propagation process of unstable rock mass as closely as possible. Simultaneous micro-vibration responses from the unstable rock mass and bedrock are recorded. The amplitude ratio and frequency ratio are calculated to validate the theoretical relationship model established in Section 2, providing foundational data for subsequent machine learning-based stability identification of unstable rock mass.

3.1. Similarity model production

The instability of unstable rock mass on slopes results from prolonged geological evolution. To capture vibration data throughout the damage-evolution-instability process of unstable rock mass, a rockfall analog model test was designed. This test progressively degraded the structural plane to induce rockfall, aiming to validate the evolution patterns of spatial vibration characteristics and the variation of key dynamic indicators in unstable rock mass.

First, a similarity model was fabricated, as shown in Figure 3(a), with a thickness of 12 cm. To ensure the reliability of model test results, research was conducted on the mix proportioning of similar materials. To simulate the characteristics of rock-like materials, high bulk density, low strength, and low modulus of deformation, a similar material was prepared using barite powder and quartz sand as aggregates, with gypsum as the binder, glycerin, a retarder, and water [17,18]. Based on physical and mechanical tests of the original rock samples, similarity theory combined with dimensional analysis was used to determine the theoretical parameters for the model. Through rock mechanics tests, the optimal mix ratio closely matching the original rock was identified. The binder-to-aggregate ratio *A* represents the mass fraction of barite powder relative to the total aggregate mass (the sum of quartz sand and barite powder mass). The binder concentration *B* denotes the mass ratio of glycerin to water. The aggregate-to-binder ratio *C* indicates the mass ratio of the total aggregate to gypsum. The physical and mechanical parameters of the original rock and the similar material are presented in Table 1.

$$\begin{cases} C_E = C_P \times C_L \\ C_\sigma = C_C = C_E \\ C_K = C_F = 1 \end{cases} \tag{6}$$

where C_ρ=1 (density ratio), C_L=100 (geometric ratio), and C_σ, C_E, C_C, C_K, C_f are the similarity ratios for stress, elastic modulus, cohesion, softening coefficient, and internal friction angle, respectively.

Table 1. Similar model proportions and mechanical parameters.

Physical parameter	ρ/(g•cm-3)	σ_t/kPa	σ_c/MPa	E/GPa	C/MPa	φ/(°)
Intact-rock parameters	2.86	956	92.26	36.85	25.19	39.72
Analog-material theoretical parameters	2.86	9.60	0.92	0.37	0.25	39.72
Analog-material experimental parameters	2.63	102.0	1.04	0.33	0.19	50.0
Ingredients	A		B		C	
Proportion	0.5		0.1		5	

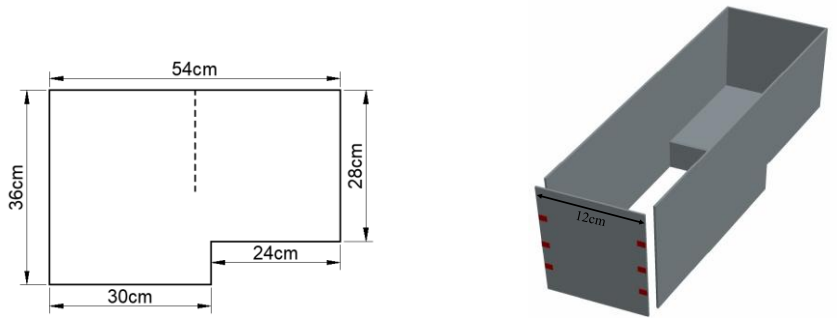

(a) Similar Model Dimensions. (b) Casting mold

Figure 3. Schematic diagram of unstable rock mass dimensions and casting model.

3.2. Experimental design

As shown in Figure 4, this is a schematic diagram of the monitoring equipment layout. The model

was secured to the ground using plaster. Contact-type vibration sensors were arranged orthogonally on the top of the unstable rock mass to collect triaxial vibration data. The *X*-axis represents the direction facing the open space, the Z-axis is the vertical direction, and the *Y*-axis is perpendicular to the *XZ* plane. White noise generators were fixed to the bedrock surface and the ground using plaster to simulate the propagation of environmental vibrations toward the unstable rock mass.

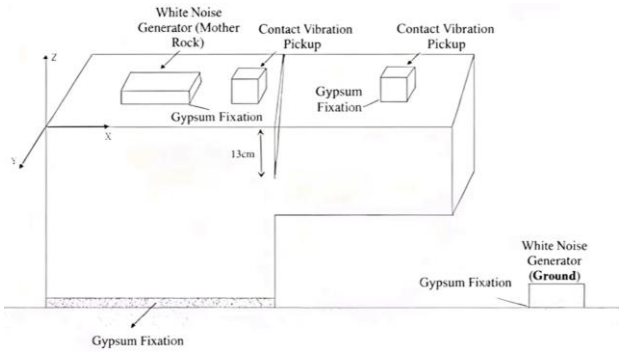

Figure 4. Monitoring equipment layout schematic diagram monitoring equipment layout schematic diagram.

The following steps were applied:

(1) We secured the model to the ground. The rear edge crack of the model was pre-cut to a position 10 cm from the rear edge. After cutting, we enabled the model to rest for 3 minutes.

(2) We initiated white noise excitation and record vibration data in the *X*, *Y*, and *Z* directions under environmental vibrations of the unstable rock mass. Each data acquisition session lasted 10 minutes.

(3) We cut downward by 0.5 cm each time, enabling the model to rest for 1 minute, and then collected data for another 10 minutes until the model became unstable.

Figure 5 shows a schematic diagram of the sensor layout and the instability process of the unstable rock mass model. The model experienced tensile failure when cut to a depth of 21 cm.

Figure 5. Instability process of a rock mass model.

3.3. Analysis of test results

The isotropic vibration time-history curves of the unstable rock mass, recorded under identical environmental excitation and plotted at the same longitudinal coordinate scale, are presented in Figures 6(a) to (c) for the *X*, *Y*, and *Z*-directions, respectively. As the rear-edge crack was progressively deepened from 0 cm to 21 cm, the structural restraint provided by the rock bridge gradually deteriorated, leading to a marked reduction in the overall stiffness of the unstable block–bedrock system. This

degradation manifested in the vibration response as a pronounced "thickening" of the time-history waveforms, characterized by a substantial increase in both peak-to-peak and root-mean-square (RMS) amplitudes. Quantitatively, the average maximum vibration amplitude of the unstable rock mass ranged from 10 to 20 times greater than that of the adjacent bedrock across all three orthogonal directions, underscoring the amplification effect induced by loss of constraint. Notably, this amplitude disparity became increasingly evident beyond a cutting depth of 16 cm.

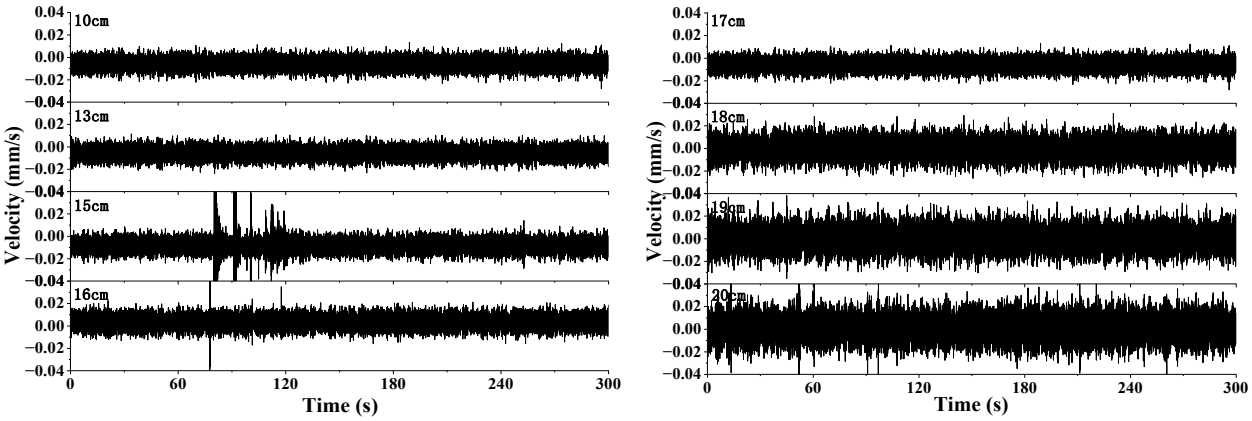

(a) X-Direction vibration of the unstable rock mass

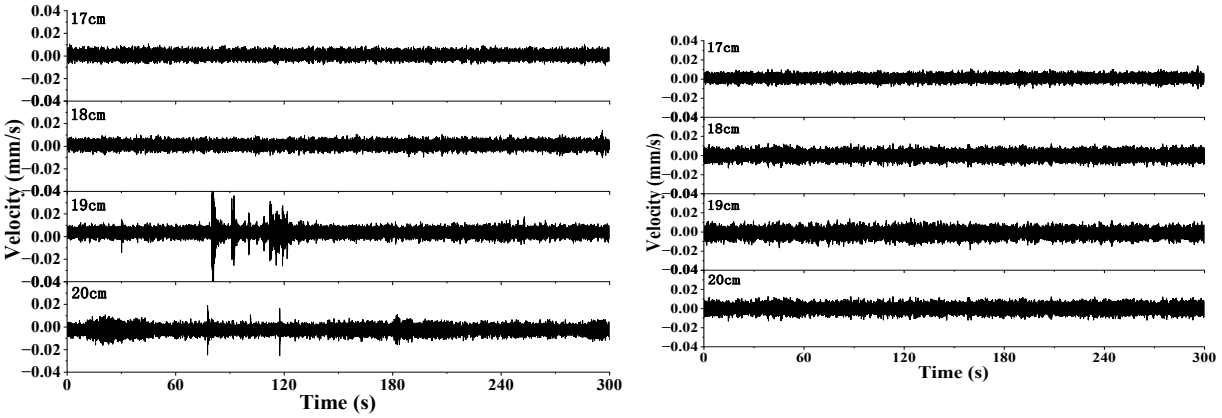

(b) Y-Direction vibration of the unstable rock mass

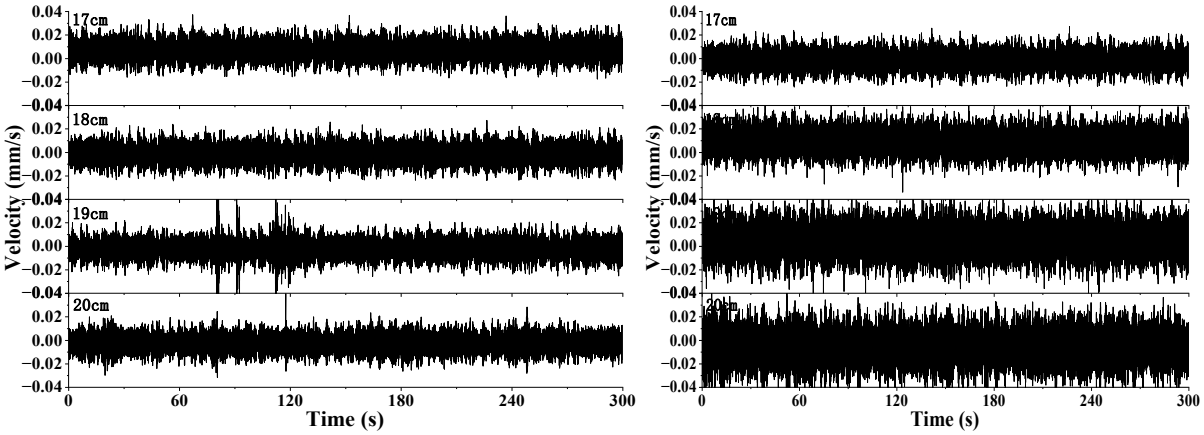

(c) Z-Direction vibration of the unstable rock mass

Figure 6. Three-dimensional vibration time history curve of a rock mass.

Figure 7 shows the isotropic vibration time-history curves of the bedrock at the same vertical coordinate scale. The vibration amplitude of the bedrock remained relatively stable throughout, with no significant changes occurring as the fracture depth increases. During the rock mass failure process, the vibration characteristics of the bedrock remained stable, showing no significant impact from fracture propagation or the failure of the rock mass.

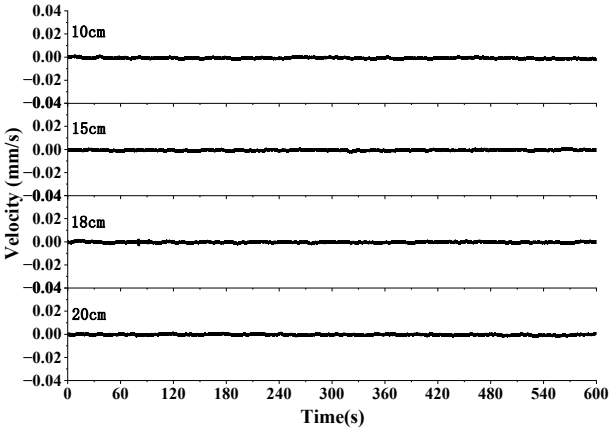

(a) X-direction vibration of the bearing rock

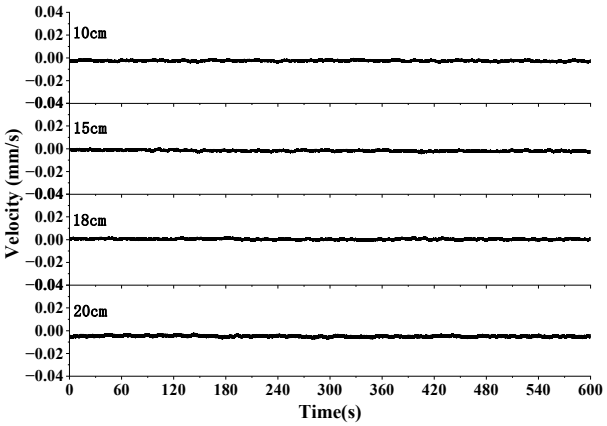

(b) Y-direction vibration of the bearing rock

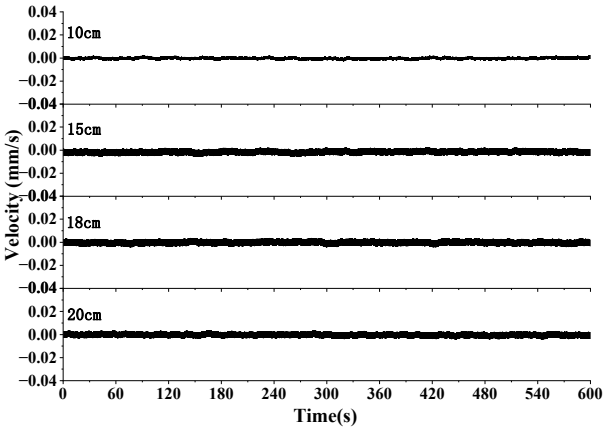

(c) Z-direction vibration of the bearing rock

Figure 7. Bearing rock vibration time history curve.

The ratio of the three-dimensional vibration standard deviation between the unstable rock mass and bedrock was defined as the amplitude ratio. The amplitude standard deviation was calculated over time intervals to minimize the impact of sporadic disturbances. This approach ensured the stability of the indicator, making it highly reliable for evaluating the vibration characteristics of unstable rock mass.

$$\begin{cases} A_i = \sqrt{x^2 + y^2 + z^2} \\ A_\sigma = \sqrt{\dfrac{\sum_{i=1}^{N} \left(A_i - \overline{A} \right)^2}{N}} \end{cases} \tag{7}$$

In the formula, A_i represents the offset distance from the origin, and A_σ denotes the amplitude standard deviation.

As crack depth increased, the amplitude ratio index showed a gradual upward trend, while the frequency ratio index exhibtied a gradual downward trend. Figure 8(a) shows the spatial amplitude ratio curve as a function of cutting depth. The indicator exhibited step changes at cutting depths of 16 cm to 17 cm and 19 cm to 20 cm. After filtering and denoising the vibration data, FFT analysis was performed to extract frequency-domain characteristics. The peak frequency ratio of the unstable rock to bedrock was used as the frequency ratio, as shown in Figure 8(b), which depicts the frequency ratio curve as a function of cutting depth. The bedrock frequency remained stable between 218 Hz and 215 Hz, while the unstable rock frequency decreased from 176 Hz to 129 Hz. The frequency ratio exhibited a step change after the cutting depth reached 16 cm.

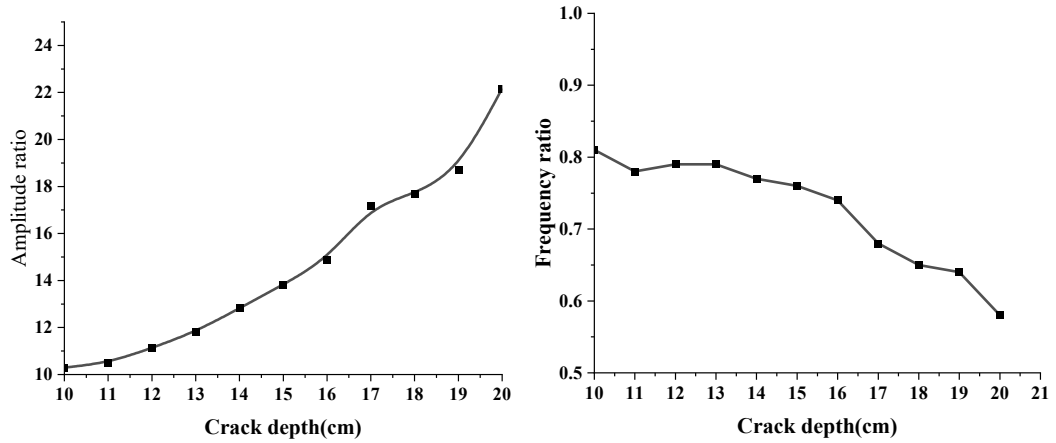

(a) Amplitude variation graph. (b) Frequency ratio variation curve chart

Figure 8. Dynamic index variation curve of the unstable rock mass.

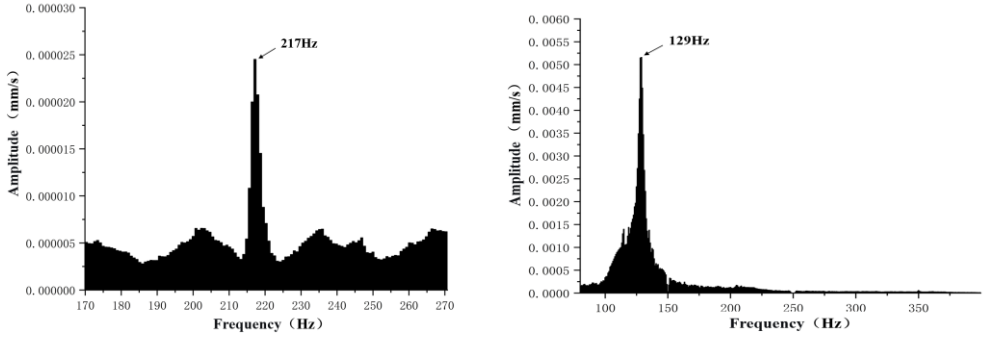

(a) Bedrock spectrum chart. (b) Spectral diagram of 20cm cutting depth for hazardous rock.

Figure 9. Comparison of spectral diagrams for unstable rock mass and bedrock.

Table 2. Amplitude ratios and frequency ratios at different fracture depths.

Crack depth	Amplitude ratio	Frequency ratio
10cm	10.30	0.81
11cm	10.50	0.78
12cm	11.13	0.79
13cm	11.83	0.79
14cm	12.82	0.77
15cm	13.83	0.76
16cm	14.90	0.74
17cm	17.15	0.68
18cm	17.67	0.65
19cm	18.70	0.64
20cm	22.17	0.58

4. Dynamic-PSO-SVM-based stability assessment of rock mass

Support Vector Machines (SVM) is a supervised learning algorithm primarily used for binary classification problems. SVM constructs an optimal hyperplane to separate data points of different classes, maximizing the margin between the two classes while searching for a linearly separable hyperplane in high-dimensional space [19]. The Particle Swarm Optimization (PSO) algorithm simulates the foraging behavior of bird flocks. Each "particle" represents a potential solution, with all particles continuously adjusting their positions and velocities within the search space based on individual experience (personal best) and group experience (global best), gradually converging toward the optimal solution [20]. Applying PSO to optimize SVM parameters (kernel function, penalty factor) improves SVM classification accuracy [21]. Based on the amplitude ratio and frequency ratio, a PSO-based SVM classification prediction model was developed for adaptive prediction of rock mass stability.

The RBF kernel function, due to its exceptional local properties, effectively maps samples to higher-dimensional spaces, thereby enhancing the model's performance in handling nonlinear problems. We selected the Gaussian radial basis function (RBF) as the kernel function, with core parameters set as follows: Learning factors $C_1 = 1.5$, $C_2 = 1.7$; population size $N = 20$; and maximum iteration count $V = 200$.

The process is as follows:

(1) Obtain the dynamic monitoring indicators of the unstable rock mass and perform normalization processing. Establish a training dataset and a testing dataset.

(2) Subsequently define the parameter search range, set the iteration count, and establish upper and lower bounds for the parameters.

(3) Determine the fitness function and calculate two evaluation metrics: Mean Squared Error and R-squared. Closer prediction results to actual outcomes indicate higher prediction accuracy.

(4) Update particle positions and velocities. Identify the current best individual fitness value based on the preceding steps. Compare this with the individual's historical fitness values and the global optimum. If the current fitness is better, save it; otherwise, continue searching.

(5) Termination criteria. The program stops when either the fitness value or iteration count meets the specified requirement.

(6) Establish a rockfall identification model using the optimized SVM parameters.

According to the Engineering Implementation, a safety factor K ranging from 1 to 1.35 is defined as an unstable state, while $K \geq 1.5$ indicates a stable state. Using the limit equilibrium method, the critical depths of rear-edge fractures at which the rock mass transitions to unstable and stable states were calculated as h=16.43 cm and h=14.21 cm, respectively. We collected 24 sets of monitoring data for the unstable rock mass. Fissure depths exceeding 17 cm were labeled unstable, while depths below 14 cm were labeled stable. Sixteen sets of data were randomly selected as training data, with the remaining eight sets used for testing.

The prediction results of the PSO-SVM training and test sets are shown in Figure 10. In this dataset, the fundamentally stable state of the rock mass was assigned a value of 0, and the unstable state was assigned a value of 1. Among the 8 test sets, the PSO-SVM classification prediction model achieves a 0% error rate, indicating that the model can accurately distinguish the stable and unstable states of the rock mass after training.

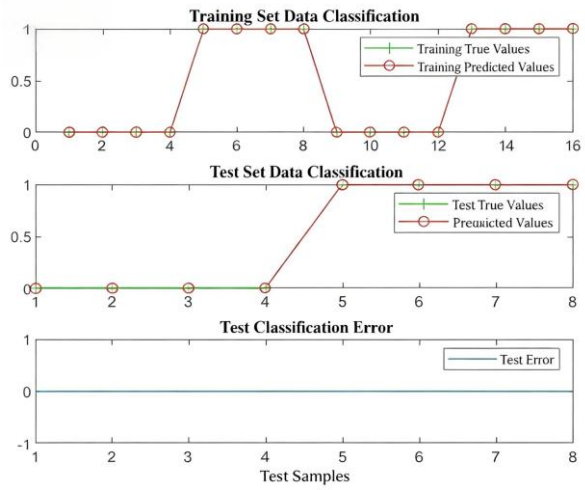

Figure 10. Dynamic PSO-SVM classification for falling rock mass stability assessment.

The classification results for rock mass stability are shown in Figure 11. The figure displays the frequency ratio on the X-axis and the amplitude ratio on the Y-axis. The classification line P represents the hyperplane constructed by the SVM, dividing the dataset into two regions: The area below the hyperplane indicates a stable state, while the area above the hyperplane indicates a sub-stable state. The results demonstrate that the PSO-SVM model successfully classifies rock mass stability states based on amplitude ratio and frequency ratio indicators.

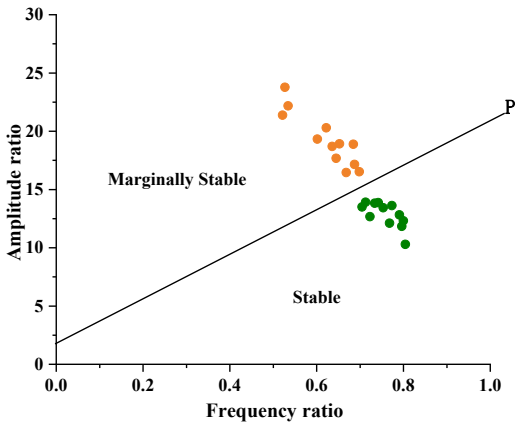

Figure 11. Classification results of rock mass stability.

Considering the scale effect, we supplemented the experimental analysis with small-scale model tests. The model volume was proportionally reduced by 0.7 times, using identical material proportions, geometric dimensions, and failure processes. A total of 24 datasets were obtained. Nine datasets were randomly selected as the test set, while the remaining 15 were added to the training set from the aforementioned experiment for training. Stability classification was conducted using different indicators (amplitude ratio and frequency ratio as dual indicators), yielding results of 78%, 78%, and 89%, respectively. By obtaining multiple dynamic indicators of the rock mass, the reliability of unstable rock mass stability identification can be effectively enhanced.

Table 3. Predictive data set of rock mass stability.

Crack depth	Amplitude ratio	Frequency ratio	Stability
Test1	18.53	0.41	Marginally Stable
Test2	9.74	0.76	Stable
Test3	12.10	0.64	Stable
Test4	16.11	0.50	Marginally Stable
Test5	9.96	0.78	Stable
Test6	10.57	0.74	Stable
Test7	16.26	0.66	Marginally Stable
Test8	9.64	0.78	Stable
Test9	16.27	0.42	Marginally Stable

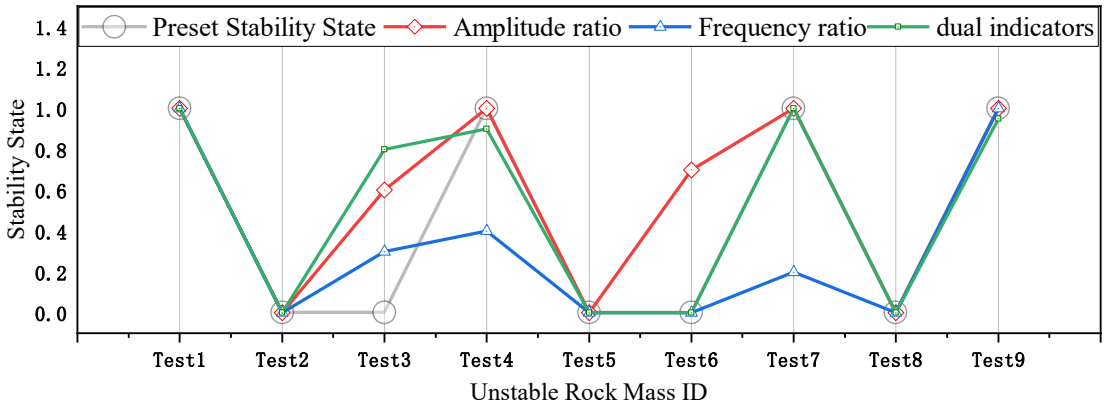

Figure 12. Comparison of prediction results.

5. Engineering applications

Using a laser Doppler vibrometer, remote vibration characteristic monitoring was conducted on the bedrock slope and two unstable rock masses at a hydropower station in the Jinsha River basin, Sichuan Province, China. Limit equilibrium analysis indicated one rock mass was stable while the other exhibited poor stability. Since laser vibrometry cannot simultaneously monitor vibration characteristics in three directions, the vibration monitoring direction in the test was selected to be as perpendicular as possible to the direction of development of the trailing edge structural surface to obtain the maximum amplitude. Micro-vibration monitoring data from the rock masses underwent filtering to calculate amplitude ratios and frequency ratios between the unstable rock mass and the stable rock mass. The results revealed that the dominant frequency of the bedrock in this area was approximately 8–9 Hz. Dynamic monitoring results for the stable rock mass closely match those of the bedrock, indicating strong coupling and high stability. The unstable rock mass exhibited significantly higher amplitudes than the bedrock and markedly different vibration frequencies. This suggests the unstable rock mass is less constrained by the bedrock and possesses greater impact energy. The dynamic evaluation results were consistent with manual quantitative assessments.

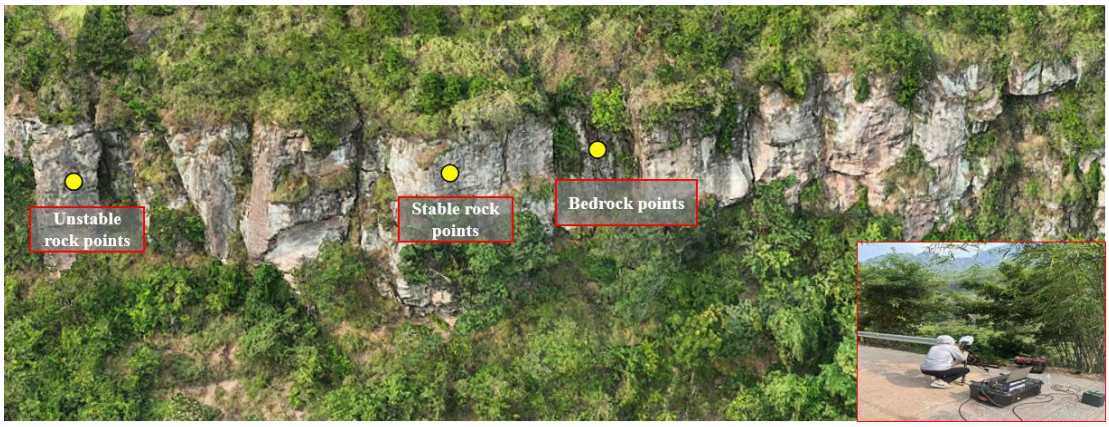

Figure 13. Laser vibration monitoring of rock mass.

Table 4. Results of kinetic indicator monitoring.

Indicator	Stable rock	unstable rock
Amplitude ratio	2.35	10.87
Frequency ratio	0.94	0.53

6. Discussion

In this study, we conducted experimental research on the rapid identification of stable and unstable rock mass by introducing a dual-indicator system of amplitude ratio and frequency ratio, combined with the PSO-SVM algorithm. The PSO-SVM-based classification model achieved identification of stable and unstable rock mass. Moreover, the discriminative efficacy of dynamic indicators was validated, providing an automated assessment method with strong anti-interference capability for engineering sites.

6.1. Analysis of nonlinear evolution processes in rock mass

The degradation of rock bridge constraint stiffness is not a continuous nonlinear process but exhibits quasi-bifurcation characteristics driven by critical events such as microfracture penetration and localized collapse, manifesting as step responses in dynamic behavior. According to the two-stage failure mechanism proposed [22], unstable rock mass progress from stability to collapse through a separation stage (partial penetration of structural planes with initial significant stiffness degradation) and an accelerated failure stage (rock bridge nearing failure with abrupt stiffness decline). These two critical points correspond to two distinct steps in the dynamic indicators: The first step marks the entry into a weakly stable state amenable to early warning, while the second step signals the imminent occurrence of irreversible instability. This pattern was validated in rock mass collapse freezing tests and a remote sensing monitoring experiment [23]. In the freezing test, monitoring results showed that the frequency monitoring index exhibited precursors to separation and accelerated failure at 50 s and 115 s, respectively. In the remote sensing monitoring test, the vibration amplitude exhibited a continuous upward trend as the strength of the structural plane decreased, followed by a sharp increase at 390 s. The amplitude increased by 2.4 and 3.1 times compared to the previous moment, respectively, triggering precursor warnings. The observed dynamic indicator step changes in this study reflect the nonlinear abrupt transition characteristics of structural plane damage in unstable rock mass at the critical point of separation failure.

6.2. Validity of relative kinetic indicator analysis

In quiet environments, ground motion excitation is relatively stable, enabling the average amplitude during monitoring to be considered the steady-state microtremor response of unstable rock mass. However, under complex environmental excitations in engineering zones, sudden strong shocks from vehicle vibrations or blasting cause abrupt changes in the amplitude response of unstable rock mass vibration signals. Therefore, relying solely on the vibration response of unstable rock mass may result in misjudging their stability. Artificial excitation was applied to the rock mass to simulate impact

vibration, and changes in the dynamic indicators of the unstable rock–bedrock system were analyzed to validate the reliability of amplitude and frequency ratio metrics. At a cutting depth of 11 cm, a pendulum was released at different angles (0°, 45°, 90°) relative to the plumb line to impact the bedrock. The resulting vibration time-history curves of the unstable rock and bedrock are shown below. With increasing impact intensity, the vibration amplitudes of the unstable rock mass and bedrock increased by factors of 10.38 and 8.16, respectively. The amplitude ratio index increased from 10.50 to 13.77, representing a 1.31-fold rise. The frequency ratio index, which reflects the inherent vibration characteristics of the rock mass and is independent of excitation magnitude, remained stable. In summary, the relative vibration index between unstable rock and bedrock effectively mitigates the influence of strong seismic shocks on their dynamic characteristics. This highlights its strong practicality for monitoring the dynamic stability of unstable rock mass under complex excitation condition.

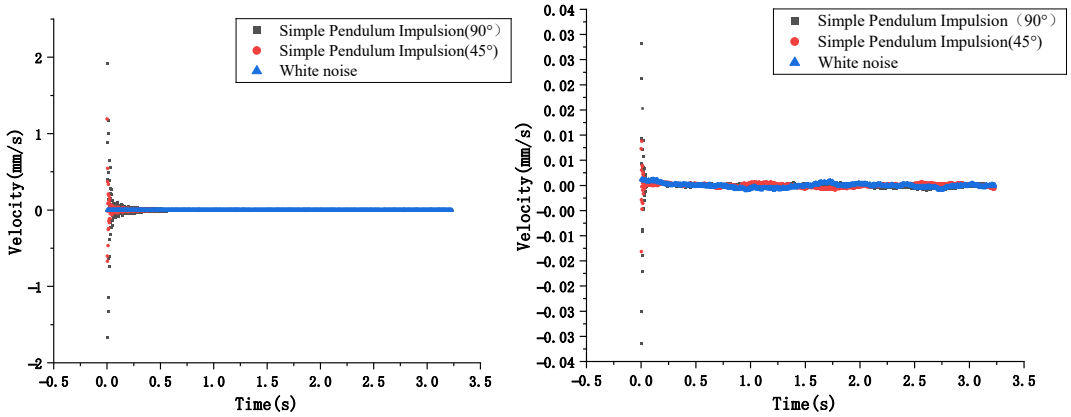

(a)Unstable rock X-Direction. (b)Bedrock X-Direction.

Figure 14. Vibration time history curves of rock mass under different excitation forces.

Table 5. Rock mass vibration time history curve.

Dynamic indicator	Simple Pendulum Impact 0°	Simple Pendulum Impact 45°	Simple Pendulum Impact 90°
Unstable rock Average Amplitude (mm/s)	0.013	0.041	0.135
Bedrock Average Amplitude (mm/s)	0.0012	0.0034	0.0098
Amplitude Ratio	10.5	12.05	13.77
Frequency Ratio	0.78	0.80	0.77

7. Conclusion

(1) Based on a simplified vibrational dynamics model, we derive the relationship between the amplitude ratio and frequency ratio indicators of unstable rock-bedrock systems and rock bridge stiffness. The frequency ratio and amplitude ratio indicators effectively reflect the differential variations in vibrational characteristics between unstable rock and bedrock.

(2) Through similar model experiments, the evolution patterns of the amplitude ratio and frequency ratio during the instability process of unstable rock mass were revealed. As the depth of the

rear-edge fissure in the falling unstable rock mass increases, the amplitude ratio gradually increases while the frequency ratio gradually decreases. Once the unstable rock mass enters the unstable phase, the indicators exhibit step-like characteristics, providing effective metrics for analyzing rock mass stability.

(3) The PSO-SVM model can accurately classify the stability state of unstable rock mass based on amplitude ratios and frequency ratios. The results demonstrate that this method effectively distinguishes stable and unstable states, reduces interference from complex environmental excitation and equipment temperature drift in vibration monitoring data, and exhibits high reliability. It enhances the dynamic evaluation method for assessing the stability state of unstable rock mass.

(4) This study has the following limitations: Undeniably, damping affects the vibration characteristics of unstable rock mass, and the damping coefficient may change during the process of fracture depth variation. We did not consider the influence of damping characteristics, and the dynamic calculation method incorporating damping characteristics requires further refinement. Although the amplitude ratio and frequency ratio demonstrated excellent stability discrimination capabilities in this study, they essentially remain low-dimensional dynamic indicator systems. Rock damage evolution is a complex, multi-scale, multi-physics-field coupled process, and single or dual indicators may struggle to comprehensively characterize intricate instability patterns (e.g., rock mass constrained by multiple structural planes). Future work will entail multidimensional dynamic indicator systems integrating time-frequency domain characteristics with spatial vibration coherence, combined with deep learning models to achieve more refined state recognition. The experiment was conducted under relatively ideal conditions with weak random noise. In real unstable rock mass subjected to complex environmental disturbances, signal fluctuations exhibit greater randomness. It may be necessary to collect data over a longer period to ensure reliability. We will continue advancing the field application of the algorithm.

Use of AI tools declaration

The authors declare they have not used Artificial Intelligence (AI) tools in the creation of this article.

Acknowledgements

The authors gratefully acknowledge the financial support from the National Natural Science Foundation of China (42477167),the National Key R&D Program of China (2023YFC3081400).

Author contributions

H.Q. Li: Conceptualization, Methodology, Experimental validation, Writing-original draft preparation. C. Zhao: Writing-review and editing. Z.N. Zou: Investigation, Supervision, Project administration, Funding acquisition. S Jiang: Experimental validation, M.W. Xie: Investigation, Supervision. Data curation. All authors have read and agreed to the published version of the manuscript.

Conflict of interest

The authors declare no conflict of interest involved in the study.

References

1. Du Y, Zhang H, Xie M, et al. (2024) A Possible Mechanism of High-Speed and Long-Distance Rockslides. *J Earth Sci* 35: 2158-2162. https://doi.org/10.1007/s12583-024-2025-5
2. Vardhan KVV, Kaushik VHSS, Sailaja K et al (2023) Detection and prediction of landslide bulnerability through case study using DInSAR technique and U-net model. 2023 5th International Conference on Smart Systems and Inventive Technology (ICSSIT), 2023: 176-182. https://doi.org/10.1109/ICSSIT55814.2023.10061077
3. Seishi, Okuzono, Kikuma, et al (1980) The method to evaluate the danger of rock-collapse at a slope by vibration measurement. *J Jpn Soc Eng Geol* https://doi.org/10.5110/jjseg.21.119
4. Burjánek J, Gassner-Stamm G, Poggi V et al (2010) Ambient vibration analysis of an unstable mountain slope. *Geophys J Int* 180: 820-828. https://doi.org/10.1111/j.1365-246X.2009.04451.x
5. Du Y, Xie M, Jiang Y, et al. (2017) Experimental Rock Stability Assessment Using the Frozen–Thawing Test. *Rock Mech Rock Eng* 50: 1049-1053. https://doi.org/10.1007/s00603-016-1138-2
6. Zhang XY, Xie MW, Zhang L et al (2023) Study on calculation model of stability coefficient of falling dangerous rock mass based on natural frequency. *Chin J Rock Mech Eng* 42: 585–593. https://doi.org/10.13722/j.cnki.jrme.2022.0361
7. Zhang XY (2023) Study on stability evaluation model of falling dangerous rock mass of slope based on natural frequency. Beijing: University of Science and Technology Beijing.
8. Zhao C, Xie MW, Du Y, et al. (2024) Spatial vibration characteristics and damage identification of toppling dangerous rock mass. *Adv Eng Sci* 56: 48–59. https://doi.org/10.12454/j.jsuese.202400255
9. Jia YC (2018) Study on Stability Model of Slope Dangerous Rock Mass Based on Dynamic Characteristics. University of Science and Technology Beijing, 2018.
10. Bottelin P, Lévy C, Baillet L et al (2013) Modal and thermal analysis of Les Arches unstable rock column (Vercors massif, French Alps). *Geophys J Int* 194: 849-858.https://doi.org/10.1093/gji/ggt046
11. Burjánek J, Gischig V, Moore J R, et al (2018) Ambient vibration characterization and monitoring of a rock slope close to collapse. *Geophys J Int* 212: 297-310. https://doi.org/10.1093/gji/ggx424
12. Kleinbrod U, Burjánek J, Fäh D (2019) Ambient vibration classification of unstable rock slopes: A systematic approach. *Eng Geol* 249: 198-217.https://doi.org/10.1016/j.enggeo.2018.12.012
13. Du Y, Xie MW (2022) Indirect method for the quantitative identification of unstable rock. *Nat Hazards* 112: 1005–1012. https://doi.org/10.1007/s11069-021-05197-4
14. He Z, Xie M, Huang Z, et al. Experimental Hazardous Rock Block Stability Assessment Based on Vibration Feature Parameters. *Adv Civ Eng* 2020: 8837459. https://doi.org/10.1155/2020/8837459
15. Wu ZX, Xie MW, Zhang XY, et al. (2024) Experimental Damage Identification of Single-Structure-Surface Rock Mass Based on Continuous Microtremors. *J Eng Sci* 46: 589-599. https://doi.org/j.issn2095-9389.2023.03.12.002.
16. He Z, Xie MW, Wu ZX, et al. (2024) Field measurement study on the pre-collapse inclination deformation characteristics of tension-cracking slope rock mass using micro-core-pile sensor. *Rock and Soil Mech* 45: 3399-3415. https://doi.org/10.16285/j.rsm.2024.0146
17. Xu C, Cui Y, Xue L, et al. (2023) Experimental study on mechanical properties and failure behaviours of new materials for modeling rock bridges. *J Mater Res Technol* 23: 1696-1711. https://doi.org/10.1016/j.jmrt.2023.01.128

18. Wang WQ, Liu YR (2020) Study on similar material ratio of rock mass based on geomechanical model test. *J Qinghai Univ* 38: 44-52.

19. Hong Y, Shao ZS, Ma L. (2017) Application of a Support Vector Machine for Analysis and Prediction of Slope Stability. *J Shenyang Jianzhu Univ* 33: 1004-1010. https://doi.org/CNKI:SUN:SYJZ.0.2017-06-006.
20. Hu MF, Ou B, Zhang CY, et al. (2023) Research on Seepage Prediction of Earth and Rockfill Dams Based on PSO-BP Model. *Water Resour Power* 41: 90-92+89. https://doi.org/10.20040/j.cnki.1000-7709.2023.20221774
21. Wang T, Li ZJ (2023) Application of PSO-SVM in Water Resources Carrying Capacity Evaluation of Heilongjiang Province. *Water Resour Power* 41: 30-33. https://doi.org/10.20040/j.cnki.1000-7709.2023.20220748
22. Du Y, Wu ZX, Xie MW, et al. (2019) Early-warning method of rock collapse and its experimental verification. *J China Coal Society* 44: 3069-3075. https://doi:10.13225/j.cnki.jccs.2018.1467
23. Du Y, Huo LC, Xie MW, Jiang YJ, Jia BN, Cong XM. (2021) Monitoring and Early Warning Experiment of Rock Collapse. *Chin J Theor Appl Mech* 53: 1212-1221. https://doi.org/10.6052/0459-1879-20-441.

AIMS Press